World Academy of Science, Engineering and Technology
International Journal of Physical and Mathematical Sciences
Vol:5, No:6, 2011

Direct Numerical Simulation of Oxygen Transfer at the Air-Water Interface in a Convective Flow Environment and Comparison to Experiments

B. Kubrak J. Wissink H. Herlina

Abstract—Two-dimensional Direct Numerical Simulation (DNS) of high Schmidt number mass transfer in a convective flow environment (Rayleigh-Bénard) is carried out and results are compared to experimental data. A fourth-order accurate WENO-scheme has been used for scalar transport in order to aim for a high accuracy in areas of high concentration gradients. It was found that the typical spatial distance between downward plumes of cold high concentration water and the eddy size are in good agreement with experiments using a combined PIV-LIF technique for simultaneous and spatially synoptic measurements of 2D velocity and concentration fields.

Keywords—Air-Water Interface, DNS, Gas Transfer, LIF.

I. Introduction

THE gas transfer through the air-water interface plays an important role in environmental and chemical engineering. One typical process is the absorption of oxygen into natural water bodies such as lakes and oceans. It is vital to sustain aquatic life. This process is controlled by interaction of molecular diffusion and turbulent transport. In nature the flow conditions are usually turbulent. It is well known that the level of turbulence plays an important role in the the gas transfer process and is the dominant driving mechanism.

Natural sources of turbulence can be classified into three major types which are surface-shear-induced turbulence (e.g. wind shear on open waters), bottom-shear-induced turbulence (e.g. in rivers) and buoyant-convective turbulence (e.g. in lakes due to surface cooling). Fig 1 shows a schematic illustration of the turbulence sources and their interaction [1].

The objective of this study is to gain a more fundamental understanding of the mechanisms that control the oxygen absorption in water dominated by convective-induced turbulence. For low soluble gases a very thin layer of gas saturated liquid will form at the interface. If the surface layer is cooled it becomes slightly heavier than the water underneath triggering a Rayleigh-Bénard instability, resulting in downwards penetration of the upper layer that is saturated with gas. Typical non-dimensional quantities of importance are the ratio of the momentum diffusivity and mass diffusivity, represented by the Schmidt number Sc , and the ratio of viscosity and thermal diffusivity, represented by the Prandtl number Pr .

Boris Kubrak and Dr. Jan Wissink are with the School of Engineering and Design, Brunel University London, United Kingdom, Kingston Lane, UB8 3PH, e-mail: Boris.Kubrak@brunel.ac.uk (see http://www.people.brunel.ac.uk/ mepgbbk1/).
Dr. Herlina is with KIT Karlsruhe, Germany.
Manuscript received March 31, 2010

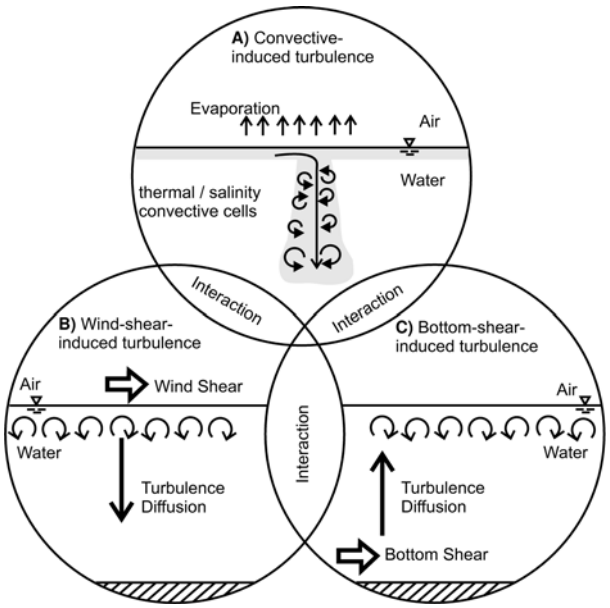

Fig. 1: Schematic illustration of the turbulence mechanisms driving gas transfer at the air-water interface in the environment. Type A is investigated in this study [1].

II. Numerical Method for Scalar Transport

The numerical scheme implemented here is a WENO (weighted essentially non-oscillatory) finite difference scheme as described by Liu, Osher and Chan [2]. WENO schemes were initially developed to capture discontinuities in the solution such as shock waves without resulting in oscillation. In a convection-diffusion problem like the gas transfer at an interface there is no discontinuity expected but high gradients may occur near the interface.

These schemes are based on cell averages and Runge-Kutta time discretisation. There is a defined reconstruction procedure which produces a high order accurate global approximation to the solution from its given cell averages.

A. The discretisation of scalar transport

In this section we describe a brief outline of the reconstruction procedure used for a scalar φ (in this case the gas concentration) when it is transported. The two-dimensional convection diffusion equation of the scalar $\varphi = \varphi(x,t)$ reads

$$\frac{\partial \varphi}{\partial t} + u\frac{\partial \varphi}{\partial x} + v\frac{\partial \varphi}{\partial y} = \left(\frac{\partial^2 \varphi}{\partial x^2} + \frac{\partial^2 \varphi}{\partial y^2}\right) \qquad (1)$$

The diffusive term on the right is discretised using a fourth-order central scheme, while the convective term is discretised using a variant of the fourth-order WENO scheme developed by Liu, Osher and Chan [2]. Below the implemented scheme is detailed only in one dimension. Generalisation to higher dimensions is straightforward.

When ignoring the diffusive term, the one dimensional variant of (1) can be rewritten as

$$\frac{\partial \varphi}{\partial t} = -u\frac{\partial \varphi}{\partial x}.$$

As we employ a staggered mesh, for the volume centred around $x = x_i$, the convective fluxes R_i^+ and R_i^- are defined by

$$\begin{aligned} R_i^+ &= \frac{a_0}{a_0+a_1+a_2}p_{i-1}(x_{i+\frac{1}{2}}) + \frac{a_1}{a_0+a_1+a_2}p_i(x_{i+\frac{1}{2}}) \\ &\quad + \frac{a_0}{a_0+a_1+a_2}p_{i+1}(x_{i+\frac{1}{2}}) \end{aligned}$$

and

$$\begin{aligned} R_i^- &= \frac{a_0}{a_0+a_1+a_2}p_{i-1}(x_{i-\frac{1}{2}}) + \frac{a_1}{a_0+a_1+a_2}p_i(x_{i-\frac{1}{2}}) \\ &\quad + \frac{a_0}{a_0+a_1+a_2}p_{i+1}(x_{i-\frac{1}{2}}) \end{aligned}$$

where

$$\begin{aligned} p_i(x) &= \frac{(x-x_i)(x-x_{i+1})}{(x_{i-1}-x_i)(x_{i-1}-x_{i+1})}\varphi_{i-1} \\ &+ \frac{(x-x_{i-1})(x-x_{i+1})}{(x_i-x_{i-1})(x_i-x_{i+1})}\varphi_i \\ &+ \frac{(x-x_{i-1})(x-x_i)}{(x_{i+1}-x_{i-1})(x_{i+1}-x_i)}\varphi_{i+1} \\ &- \frac{(x_i-x_{i-1})\varphi_{i+1} - (x_{i+1}-x_{i-1})\varphi_i + (x_{i+1}-x_i)\varphi_{i-1}}{12(x_{i+1}-x_i)} \end{aligned}$$

are quadratic Lagrange interpolations of the scalar to the faces of the volume combined with a smoothing term at the right. Using the obove, depending on the signs of $u_{i-\frac{1}{2}}$ and $u_{i+\frac{1}{2}}$, we have four possible ways to calculate $L_i(\varphi) = \left(-u\frac{\partial \varphi}{\partial x}\right)|_{x_i}$:

$$\begin{aligned} u_{i+\frac{1}{2}} > 0, u_{i-\frac{1}{2}} > 0 : L_i(\varphi) &= -\frac{u_{i+\frac{1}{2}}R_i^+ - u_{i-\frac{1}{2}}R_{i-1}^+}{x_{i+\frac{1}{2}} - x_{i-\frac{1}{2}}} \\ u_{i+\frac{1}{2}} > 0, u_{i-\frac{1}{2}} < 0 : L_i(\varphi) &= -\frac{u_{i+\frac{1}{2}}R_i^+ - u_{i-\frac{1}{2}}R_i^-}{x_{i+\frac{1}{2}} - x_{i-\frac{1}{2}}} \\ u_{i+\frac{1}{2}} < 0, u_{i-\frac{1}{2}} > 0 : L_i(\varphi) &= -\frac{u_{i+\frac{1}{2}}R_{i+1}^- - u_{i-\frac{1}{2}}R_{i-1}^+}{x_{i+\frac{1}{2}} - x_{i-\frac{1}{2}}} \\ u_{i+\frac{1}{2}} < 0, u_{i-\frac{1}{2}} < 0 : L_i(\varphi) &= -\frac{u_{i+\frac{1}{2}}R_{i+1}^- - u_{i-\frac{1}{2}}R_i^-}{x_{i+\frac{1}{2}} - x_{i-\frac{1}{2}}} \end{aligned}$$

The time discretisation of WENO schemes is implemented by a third order Runge-Kutta-type method developed by Shu and Osher [3]. The third order Runge-Kutta (RK3) time discretisation scheme reads,

$$\begin{aligned} \varphi_i^{(1)} &= \varphi_i^n + \Delta t L_i(\varphi_i^n) \\ \varphi_i^{(2)} &= \frac{3}{4}\varphi_i^n + \frac{1}{4}\varphi_i^{(1)} + \frac{1}{4}\Delta t L_i(\varphi_i^{(1)}) \\ \varphi_i^{(n+1)} &= \frac{1}{3}\varphi_i^n + \frac{2}{3}\varphi_i^{(2)} + \frac{2}{3}\Delta t L_i(\varphi_i^{(2)}) \end{aligned} \quad (2)$$

In the above, the weights for the convex combination of quadratic Lagrange interpolation polynomials are given by,

$$\begin{aligned} a_0 &= \frac{1}{12(\varepsilon - IS_i)^3} \\ a_1 &= \frac{1}{2(\varepsilon - IS_{i+1})^3} \\ a_2 &= \frac{1}{4(\varepsilon - IS_{i+2})^3} \end{aligned} \quad (3)$$

where $\varepsilon = 10^{-9}$ and the smoothness indicator IS_i is defined by

$$\begin{aligned} IS_i = \frac{1}{2}&((\varphi_{i-1}-\varphi_{i-2})^2 + (\varphi_i - \varphi_{i-1})^2) \\ &+ (\varphi_1 - 2\varphi_{i-1} + \varphi_{i-2})^2. \end{aligned} \quad (4)$$

In the case of using three quadratic interpolations fourth-order accuracy can be achieved. Note that the weights given to the interpolating polynomials depend on the local smoothness of the solution. In regions where the solution is smooth the polynomial are given higher weights than in regions near discontinuities (shocks) or sharp gradients (like the gas concentration near the interface in this case).

The two-dimensional incompressible Navier-Stokes equations are solved on a staggered mesh. The convective terms are solved using a fourth-order accurate kinetic energy conserving discretisation while the diffusive terms are solved using a fourth-order central method. For the time-integration a second-order Adams-Bashworth method is employed. A detailed description of the method can be found in [6]. The Boussinesq approximation was employed to model the buoyancy due to temperature differences in the water. A linear relationship between temperature and density was assumed.

III. Results

The results presented here are from 2D simulations that are carried out in order to perform parameter studies. A quadratic 2D domain was chosen with edge length of 10 cm. The gridsize is $n_x = 800$ and $n_y = 300$ whereas the mesh was refined near the top where the concentration boundary layer will form. A mesh refinement study where the mesh was refined by factor 1.5 and 2 found no significantly higher resolution in gas concentration and flow structures. There were periodic boundary conditions on the sides and a free slip

condition at the bottom. After $t = 10$ time units random disturbances of 1% were added to the temperature field. This is in order to avoid the triggering of the instability to depend on the mesh size or numerical round off error. The same random field was used for all simulations.

A. Gas Concentration Field

Fig. 2 shows a sequence of the non-dimensional gas concentration contour plots that visualises the development of the flow. At the initial stage (Fig. 2a) very fine plumes from the saturated thin top layer start to penetrate the lower regions which have low concentration levels. Some detachments are visible later but the fine structures of high concentration show almost no numerical diffusion even though the Schmidt number is very high. The WENO-Scheme is able to resolve the high gradient in relatively small spaces and conserves the fine structures well. The Schmidt number is $Sc = 500$ which is equivalent to the solution process of oxygen into water.

B. Comparison to Experiments

The oxygen concentration field was measured in experiments at KIT by a Laser Induced Fluorescence (LIF) method. This optical measurement technique has been developed by Vaughan & Weber [4]. The method enables an instantaneous 2D visualisation with good resolution of the dissolved oxygen concentration [5]. The experiments were performed in a tank where the surface temperature was 3°C lower than the bulk temperature of the water.

Fig. 3 shows a comparison of 2D-LIF images to our 2D DNS results. Note that the DNS results show the top section of the domain that have the same dimension as the LIF-maps. The whole domain was much larger so the sides and bottom in these plots can be considered as open boundaries. For reasons of better comparison the timescale was set to $t = 0s$ from the moment when the instability began. Though the numerical results are only 2D, whereas the real problem is of course 3D, there is still a very good qualitative agreement with the experiment. Especially between $t = 16s$ and $t = 28s$ the spatial distance between high concentration plumes and the size of the eddies is very similar in the experiment and the simulation.

IV. Conclusion and Outlook

The DNS results show similar flow structures and eddy size as seen in the experiment. The WENO scheme proved to be a successful method to resolve a scalar transport problem with a low diffusivity (and therefore high gradient) such as the oxygen concentration in water. Very fine plumes of high oxygen concentration were found to penetrate the deeper regions and their structure was well maintained. The size and spatial distance between these plumes and their development in time were in good agreement with the experiments performed [7].

Further work will involve a linearity study to see the influence of higher temperature differences between the top surface and the bulk on the distance between plumes and the spatial dimension of the eddy structure. Subsequently the investigation of the problem in full 3 dimensional simulations is planned.

References

[1] Herlina, *Gas Transfer at the Air-Water Interface in a Turbulent Flow Environment*, Universitätsverlag Karlsruhe, ISBN 3-937300-74-0, 2005.

[2] X. Liu, S. Osher and T. Chan, *Weighted Essentially Non-oscillatory Schemes*, Journal of Computational Physics 115, 200-212, 1994.

[3] C-W. Shu and S. Osher, *Efficient Implementation of Essentially Non-oscillatory Shock-Capturing Schemes*, Journal of Computational Physics 77, 439-471, 1988.

[4] W.-M. Vaughan and G. Weber, *Oxygen quenching of pyrenebutyric acid fluorescence in water, a dynamic probe of the microenvironment.* ,Biochemistry 9, 464-473, 1970.

[5] T. Muensterer and B. Jaehne, *LIF measurement of concentration profiles in the aqueous mass boundary layer*, Experiments in Fluids 25, 190-196, 1998.

[6] J.G. Wissink, *On unconditional conservation of kinetic energy by finite-difference discretizations of the linear and non-linear convection equation*, Computers and Fluids, Vol. 33, No 2, 315-343, 2004.

[7] G.H. Jirka, H. Herlina and A. Niepelt, *Gas transfer at the airwater interface: experiments with different turbulence forcing mechanisms*, Experiments in Fluids, Vol. 49, No. 1, 319-327, 2010.

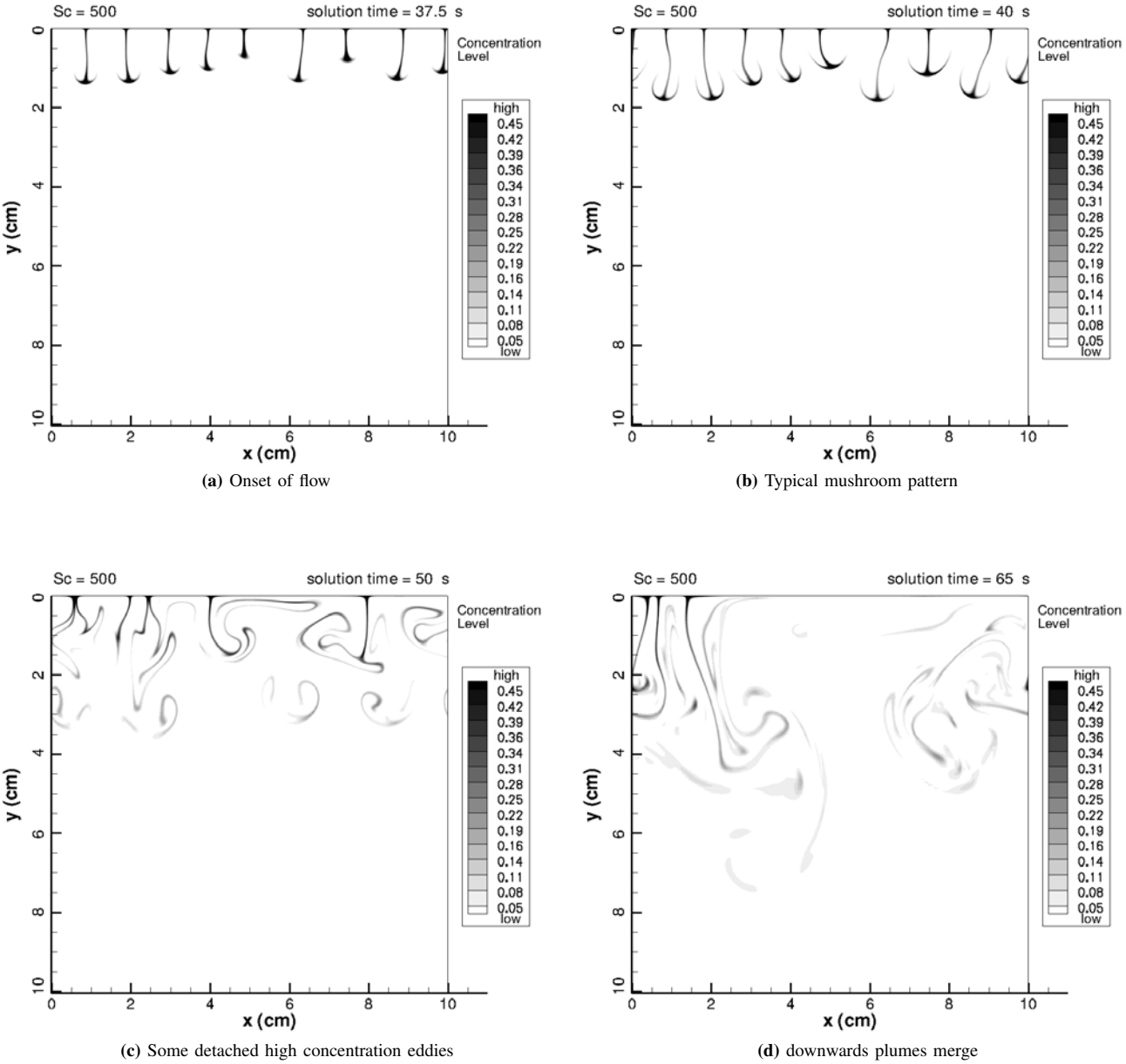

(a) Onset of flow

(b) Typical mushroom pattern

(c) Some detached high concentration eddies

(d) downwards plumes merge

Fig. 2: A sequence of oxygen concentration contour maps visualizing the onset of the Rayleigh-Bénard instability subsequent mixing. 800 x 300 gridpoints. The surface temperature $T_S = 17$ °C. The bulk temperature $T_0 = 20$ °C

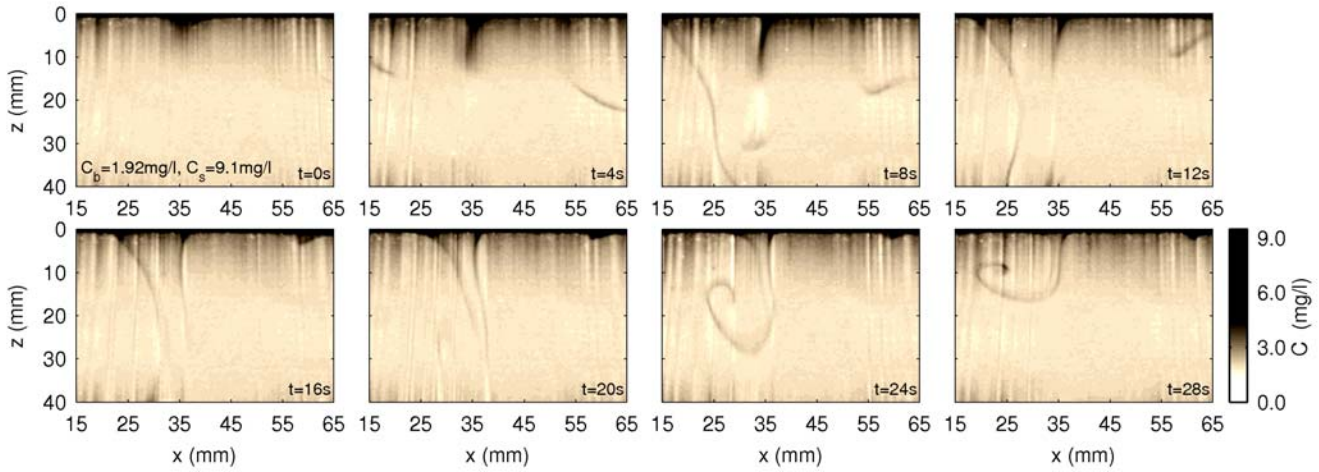

(a) Experimental Results

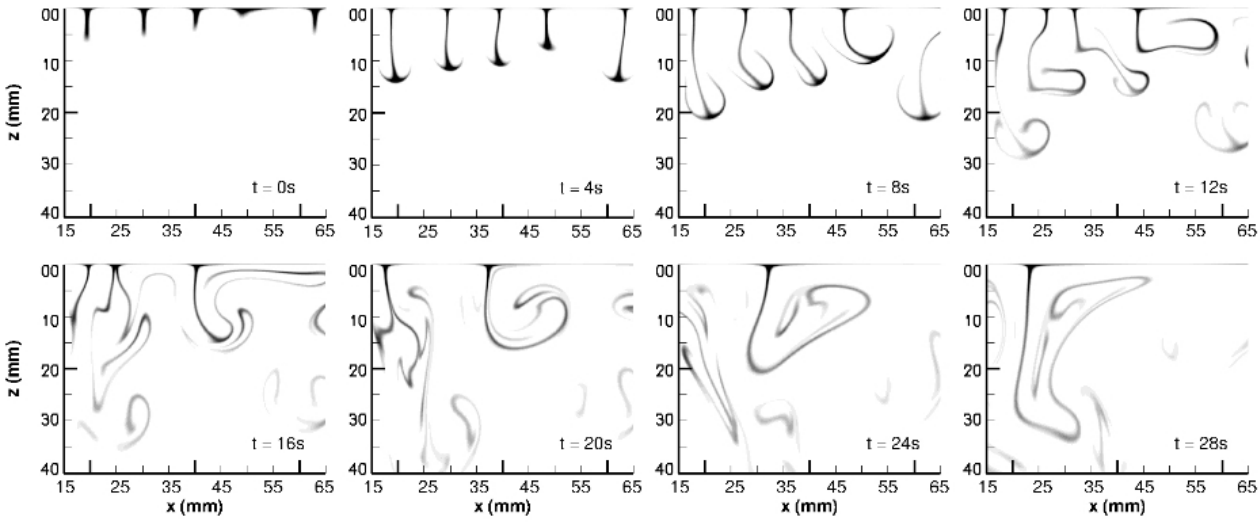

(b) Numerical Results

Fig. 3: Comparison of flow structures. High Oxygen concentration plumes of LIF measurements (Fig. 3a) [7] and DNS results (Fig. 3b). In both cases the surface temperature is 3 °C colder than the bulk temperature